

**A Point Acoustic Device Based on Aluminum Nanowires**

Journal:	<i>Nanoscale</i>
Manuscript ID	NR-ART-10-2015-006999.R2
Article Type:	Paper
Date Submitted by the Author:	17-Dec-2015
Complete List of Authors:	Xie, Qian-Yi; Institute of Microelectronic, Tsinghua University, Ju, Zhen-Yi; Tsinghua University, Institute of Microelectronic Tian, He; Tsinghua University, Institute of Microelectronic Tao, Lu-Qi; Tsinghua University, Institute of Microelectronic Chen, Yuan-Quan; Tsinghua University, Institute of Microelectronic Mohammad, Mohammad Ali; Tsinghua University, Institute of Microelectronics Xue, Qing-Tang; Tsinghua University, Institute of Microelectronics Zhang, Xue-Yue; Tsinghua University, Institute of Microelectronic Yang, Yi; Tsinghua University, Institute of Microelectronics Ren, Tian-Ling; Tsinghua University, Institute of Microelectronics

A Point Acoustic Device Based on Aluminum Nanowires

Qian-Yi Xie,^{a, c, Δ} Zhen-Yi Ju,^{b, c, Δ} He Tian,^{a, c} Qing-Tang Xue,^{a, c} Yuan-Quan Chen,^{a, c} Lu-Qi Tao,^{a, c} Mohammad Ali Mohammad,^{a, c} Xue-Yue Zhang,^{a, c}, Yi Yang,^{a, c} Tian-Ling Ren^{*a, c}

^a Institute of Microelectronics, Tsinghua University, Beijing 100084, China

^b Department of Physics, Tsinghua University, Beijing 100084, China

^c Tsinghua National Laboratory for Information Science and Technology (TNList), Tsinghua University, Beijing 10084, China.

*Email: RenTL@tsinghua.edu.cn

Δ Both authors contributed equally to this work.

A point Electrical Thermal Acoustic (ETA) device based on aluminum nanowire contacts is designed and fabricated. Interdigitated structural aluminum nanowires are released from the substrate by Inductively Coupled Plasma Reactive Ion Etching (ICP-RIE). By releasing the interdigitated structure, the nanowires contact each other at approximately 1 mm above the wafer, forming a Point Contact Structure (PCS). It is found that the PCS acoustic device realizes high efficiency when a biased AC signal is applied. The PCS acoustic device reaches a sound pressure level of as high as 67 dB at a distance of 1cm with 74mW AC input. The power spectrum is flat, ranging from 2 kHz to 20 kHz with a less than ± 3 dB fluctuation. The highest normalized Sound Pressure Level (SPL) of the point contact structure acoustic device is 18dB higher than the suspended aluminum wire acoustic device. Comparisons between the PCS acoustic device and the Suspended Aluminum Nanowire (SAN) acoustic device illustrate that the PCS acoustic device has a flatter power spectrum within the 20 kHz range, and enhances the SPL at a lower frequency. Enhancing the response at lower frequencies is extremely useful, which may enable earphones and loudspeaker applications within the frequency range of the human ear with the help of pulse density modulation.

A Introduction

Acoustic devices in common use now-a-days are usually based on moving coils^{1, 2}, piezoelectric materials³⁻⁷ or electrostatic structures^{8, 9}. For devices based on moving coils, the coils are driven by an electrical signal. The motion of the coils causes connected membranes to vibrate and thereby sound waves are generated. For piezoelectric-based and electrostatic-based devices, the vibrations are generated by an AC signal applied to the structures, the piezoelectric membrane, and the capacitor, respectively. There are two drawbacks of these three types of speakers. One of the shortcomings is the existence of resonant peaks in the power spectra^{1, 3, 8} for all three types. With resonant peaks, it is impossible to achieve an absolutely flat power spectrum. For coil-based acoustic sources, the typical fluctuation range of the SPL^{1, 2} is ± 20 dB. For piezoelectric-based or electrostatic-based devices, the typical value is ± 30 dB³⁻⁷ and ± 10 dB^{8, 9}, respectively. It is necessary to fabricate a high performance acoustic device with a lower range of fluctuation. The other drawback of contemporary acoustic devices is the poor fabrication process compatibility. The fabrication process of most moving coil transducers are not Complementary Metal Oxide Semiconductor (CMOS) compatible. With a non-CMOS process, the contemporary acoustic devices cannot be integrated with peripheral circuits. These shortcomings result in an uneven power spectra of popular transducers, and non-integrate able features of most coil-based acoustic devices.

Most ETA devices could be both CMOS-compatible and scalable¹⁰, enabling integrating extremely small transducers with

peripheral circuits. ETA devices based on silicon and other CMOS-related materials can be fabricated by CMOS technology such as photolithography, chemical vapor deposition, physical vapor deposition, standard cleaning and etching processes, etc. An ETA device could theoretically achieve an absolutely even spectrum as it does not contain any resonant component.

The ETA effect was first demonstrated systematically in 1898 by F. Braun¹¹, where both alternating and direct current were applied to a bolometer. After the ETA effect was carefully investigated by Arnold and Crandall¹² in 1917, few investigations were conducted on this topic until H. Shinoda et al.¹³ demonstrated the ultrasonic emission of porous silicon in 1999. Since then, several kinds of ETA devices based on different materials were demonstrated. ETA devices were made by porous silicon and aluminum membrane¹³, aluminum nanowires¹⁴, graphene¹⁵⁻¹⁸, carbon nanotubes¹⁹⁻²³, indium tin oxides²⁴, silver nanowires²⁵, gold nanowires²⁶, crystalline silicon²⁷, etc. Devices based on each kind of material features different power spectrum shapes and different highest normalized SPL. These discrepancies are caused by differences in the shape of the structure, Heat Capacity Per Unit Area (HCPUA), heat conductivity and fabrication process^{12, 28}. Several theoretical works have also been done on ETA devices²⁸⁻³³.

The scalability, ability of integration and theoretical power spectrum flatness of the ETA device has attracted a lot of attention in both theoretical and experimental domains; however, its efficiency remains low and the power spectrum is uneven at low frequencies. This work demonstrates a point ETA device based on

PCS, which could enhance the performance of ETA device by solving these problems. Fig. 1 demonstrates the concept of a PCS acoustic devices and Fig. 2 shows the structure of the PCS acoustic devices. Power spectra of both PCS acoustic devices and SAN acoustic devices are compared. The PCS acoustic device is fabricated on a wafer-scale and the reliability and uniformity of the fabrication process is tested.

The rest of this article is assembled as described below: Part II demonstrates a theoretical method to characterize the performance of the PCS acoustic device and compares it with the performance of the SAN acoustic device. Part III describes the fabrication processes of both the PCS acoustic device and the SAN acoustic device and compares the effect of different substrate materials to the formation of PCS. Part IV describes the test results and compares the performance between the PCS acoustic device and the SAN acoustic device. Part V compares the PCS acoustic device and the SAN acoustic device by showing simulation results. Finally, the conclusions are provided in part VI.

B Theory of the PCS acoustic device

The ETA effect could be described as four serialized stages¹². The first stage is a joule heating process. When an AC signal is applied, periodic heating of nanowires takes place, resulting in periodic temperature variation of the device surface. The second stage is a heat transfer process. The propagation of periodically varying temperature from nanowires into the surrounding fluid forms a temperature wave. The third stage is a fluid expansion and contraction process. The last stage is a sound emission process. The amplitude of the temperature wave falls rapidly and the sound wave evolves from the pressure oscillation.

The first and second stages are determined by the character of the nanowires and the fluid, including HCPUA and heat conductivity of the nanowires and the efficiency of convection between nanowires and the fluid^{12, 28, 34}. Before considering the heat propagated into fluid, the distribution of nanowire temperature is calculated by Eqn (1)³⁴.

$$T = T_0 \exp(-k_1 r) \times \sin(\omega t - k_1 r) \quad (1)$$

In Eqn (1), $k_1 = \sqrt{\frac{\pi f}{\alpha_v}}$ and $\alpha_v = \frac{k}{\rho C_v}$. ω is the circular

frequency of signal, f is the frequency of signal, T_0 is the temperature of source, k is the conductivity of fluid, $C_{v,fluid}$ is the heat capacity of fluid at constant volume, and ρ is the density of fluid. The equation has been modified using three dimensional spherical coordinates. The thermal energy of the

system is composed of two separate parts. One part is the energy of the fluid and the other part is the energy of the sound source. Furthermore, the fluid is considered as the combination of fluid outside the device and fluid inside the device²⁸. The thermal energy of the fluid outside the device is calculated by Eqn (2).

$$\frac{dQ_{fluid, outside}}{dt} = \int_0^\infty \rho A C_{v, fluid} T \omega \cdot 2\pi r^2 dr \quad (2)$$

By calculating the integration, the thermal energy of the fluid outside the device could be described by a more explicit differential equation, shown by Eqn (3).

$$\frac{dQ_{fluid, outside}}{dt} = \rho A C_{v, fluid} T_0 \omega \cdot \frac{2\pi}{\sqrt{2} k_1^3} \sin\left(\omega t - \frac{3\pi}{4}\right) \quad (3)$$

In Eqn (4) and Eqn (5), $\dot{Q}_{fluid, PCS}$ and ξ_{PCS} are defined to simplify the equations.

$$\dot{Q}_{fluid, PCS} \equiv \dot{Q}_{fluid, outside} + \dot{Q}_{fluid, inside} \quad (4)$$

$$\xi_{PCS} \equiv \frac{\rho_s C_s d_s}{\rho C_{v, fluid} \cdot \left(\sqrt{2} \pi \left(\frac{\alpha_v}{\pi f} \right)^{3/2} + d_{gap, PCS} \right)} \quad (5)$$

In Eqn (5), $d_{gap, PCS}$ is the distance between contact points and the substrate, ρ_s is the density of source, C_s is the heat capacity of source and d_s is the thickness of the source. Using Eqn (1) ~ Eqn (5), the relationship between the applied power and the thermal energy propagated into the fluid is calculated.

$$\dot{Q}_{fluid, PCS} = \frac{1}{2} \cdot \frac{1}{1 - \sqrt{2} \xi_{PCS} + \xi_{PCS}^2} \cdot P_e \quad (6)$$

In Eqn (6), P_e is the power of the input signal. The third and fourth stages are based on the state equation of fluid. The relationship between the sound pressure and the thermal energy of the fluid is described by Eqn (7)²⁸.

$$p_{rms} = \frac{f}{2\sqrt{2} C_p T_0 r} \times \dot{Q}_{fluid} \quad (7)$$

In Eqn (7), C_p is the heat capacity of fluid at constant pressure. Considering all these four stages and the structure of the PCS acoustic device, the equation of the sound pressure is demonstrated by Eqn (8), showing a direct relationship between frequency and sound pressure. The essential point of the calculation is that the phase delay has been considered which gives out a different result.

$$P_{rms,PCS} = \frac{1}{2} \cdot \frac{1}{1 - \sqrt{2}\xi_{PCS} + \xi_{PCS}^2} \cdot \frac{f}{2\sqrt{2}C_p T_0 r} \cdot P_e \quad (8)$$

The performance of the SAN acoustic device is also calculated. ξ_{AW} is defined in Eqn (9) to simplify the equations:

$$\xi_{AW} \equiv \frac{\rho_s C_s d_s}{\rho C_{v,fluid} \cdot \left(\frac{1}{\sqrt{2}} \left(\frac{\alpha_v}{\pi f} \right)^{1/2} + d_{gap,AW} \right)} \quad (9)$$

where $d_{gap,AW}$ is the distance between the nanowires and the substrate. The thermal energy propagated into the fluid is calculated in Eqn (10).

$$\dot{Q}_{fluid,AW} = \frac{(2 + 2\sqrt{2}\xi_{AW} + 2\xi_{AW}^2 + \sqrt{2}\xi_{AW}^3)}{4(1 + \sqrt{2}\xi_{AW} + \xi_{AW}^2)^2} \cdot P_e \quad (10)$$

Since the structure is totally different to the PCS acoustic device, the results are fundamentally different.

The relationship between the sound pressure and the thermal energy of the SAN acoustic device is the same as it is of the PCS acoustic device. Thermal conversion ratio (TCR) η is defined as $\eta = \dot{Q}_{fluid} / P_e$. Ratio of the pressure of two structures is calculated by Eqn (11).

$$\frac{P_{rms,PCS}}{P_{rms,AW}} = \frac{\eta_{PCS}}{\eta_{AW}} = \frac{1/2(1 - \sqrt{2}\xi_{PCS} + \xi_{PCS}^2)}{(2 + 2\sqrt{2}\xi_{AW} + 2\xi_{AW}^2 + \sqrt{2}\xi_{AW}^3) / 4(1 + \sqrt{2}\xi_{AW} + \xi_{AW}^2)^2} \quad (11)$$

In Eqn (11), $\rho = 0.8826 \text{ kg/m}^3$, $k = 0.03365 \text{ W/m}\cdot\text{C}$, $C_{v,fluid} = 1014 \text{ J/kg}\cdot\text{C}$, $\rho_s = 2700 \text{ kg/m}^3$, $C_s = 880 \text{ J/kg}\cdot\text{C}$,

$d_s = 30 \text{ nm}$, $d_{gap,AW} = 10 \mu\text{m}$, $d_{gap,PCS} = 1 \text{ mm}$. The frequency is set at 20 kHz. The TCR of each structure is calculated, giving out $\eta_{AW} = 0.084$ and $\eta_{PCS} = 0.519$. The ratio of pressure generated by the two acoustic sources is 6.655. The highest normalized SPL of the PCS acoustic device is 16.5 dB higher than the highest normalized SPL of the SAN acoustic device.

C Method

This part is divided into three sections. Section A describes fabrication processes of both PCS acoustic devices and SAN acoustic devices. Section B shows how the substrate material affects the device fabrication and illustrates how the PCS is formed by strain releasing. Section C describes the test method.

A Fabrication Process

The fabrication of both PCS acoustic devices and SAN

acoustic devices are CMOS compatible [Fig. 3]. This important feature for ETA devices enables future integration of sound sources with peripheral circuits and also the scaling down of device size. As shown, the PCS acoustic device goes through five steps before it is tested. The device is based on an n-type 2-inch wafer with a 500 nm thick silicon oxide layer. The wafer is cleaned using acetone and ethanol, dried on a hot plate, and then spun-cast using NRZ-6000 PY photoresist. Subsequently, the wafer is patterned using a 2-inch mask aligner and developed using RD-6 for 1 min. The developed wafer is sputtered with 30 nm aluminum afterwards and then the lift-off process is done in an ultrasonic cleaner using acetone for 5 min. Before the lift-off process, wafers are placed horizontally in N_2 atmosphere for 24 hours to let the strain between the aluminum layer and the silicon oxide layer release, avoiding unwanted damage of nanowires caused by the strain. After the lift-off process, the exposed silicon oxide is etched away by SF_6 and O_2 using ICP-RIE method. After the silicon oxide is etched, the silicon underneath is etched by SF_6 using the same equipment and method. The SAN acoustic device shares the same fabrication process as the PCS acoustic device, except differences in masks. Optical microscope images of PCS devices after lift-off process are shown [Fig. 4]. The width of each nanowire is about 2 μm while the thickness is 30 nm. For the PCS acoustic device, nanowires are released as shown in the SEM image [Fig. 5]. Each contact point is a point sound source. The area of the contact point is determined by the scale of nanowires together with the twisting angle of the contact. Considering the width and thickness of nanowires, the smallest possible contact area is $30 \times 30 \text{ nm}^2$ while the largest is $2 \times 2 \mu\text{m}^2$. With a contact area of $30 \times 30 \text{ nm}^2$, a PCS acoustic device could be considered as a 0-D acoustic device, comparing to other sound sources. Photos and SEM images of the SAN acoustic device after lift-off are also shown [Fig. 4, 5]. The length of a single nanowire is 100 μm and the width and the thickness are the same as the width and the thickness of the PCS acoustic device.

B Formation of PCS

Different substrates have been used to investigate the formation of PCS. ETA devices are fabricated based on silicon wafer with 500 nm thick silicon oxide (Sample A), and silicon wafer with no oxide (Sample B). Both samples go through five steps mentioned in Section A before they are tested. Although the duration, the power, and the air flow density of the etching process are adjusted for sample B, PCS is not formed. Comparing differences between samples A and B, we stated that the formation of PCS is due to the existence of silicon oxide layer between the aluminum nanowires and the silicon substrate. The main difference between the two samples is the existence of the

silicon oxide layer. For sample A, strain exists between aluminum and silicon oxide, and between silicon oxide and silicon. For sample B, strain exists only between aluminum and silicon. As the formation of silicon oxide is based on thermal oxidation of silicon, the strain between the silicon substrate and the silicon oxide layer is too large to be ignored. Fig. 5 illustrates the formation of PCS and the effect of strain on the formation. As shown in Fig. 5, the first stage is the etching of silicon oxide. Since the technique adopted is not absolutely anisotropic, the exposed silicon oxide is etched heavily while the part under nanowires is slightly etched, forming a trapezoid structure (Marked in Fig. 5b). The second stage is the over etching of silicon. Considering the isotropy and selectivity of the process and the etchant respectively, the silicon oxide is protected while the silicon is etched to a trapezoid structure (Marked in Fig. 5d). As the etching continues, the silicon under silicon oxide is etched away, releasing the silicon oxide together with nanowires from the substrate. The release is accompanied by curling of the nanowires. This curling effect is due to the continuous releasing of strain between the silicon oxide layer and the silicon substrate. The strain-caused distortion of silicon oxide eventually causes the attached nanowires to curl, forming the PCS.

C Test Setup

Both the PCS acoustic device and the SAN acoustic device are tested under the same equipment setting and using the same method. The acoustic device is tested in frequency-domain from 500 Hz to 20 kHz. The input sinusoidal signal is generated by an Agilent 35670A spectrum analyzer and the sound generated is collected by a B&K receiver (Model 4134). The equipment setting is shown [Fig. 6]. The sound collecting distance is 1 cm from the sound emitting position, i.e., 1 cm from the wafer for the SAN acoustic device, and 1.1 cm from the wafer for the PCS acoustic device. The frequency of AC signal is swept from 500 Hz to 20 kHz, collecting 400 points during 40 seconds. A 5 V DC bias is applied to handle the double frequency effect⁷. The peak to peak value of the AC signal measures 10 V.

D Results and Discussion

SPL and power spectra comparison between PCS acoustic devices and SAN acoustic devices are made [Fig. 7]. Comparison of the SPL and power spectra between two types of devices shows two significant differences, firstly, the flatness of the spectra, and secondly, the SPL at low frequency range down to 500 Hz. The main criteria we adopted for performance of acoustic devices are ± 3 dB fluctuation range and the highest normalized SPL. A wider range and a normalized higher SPL both indicate a better device. For PCS acoustic device, the ± 3 dB fluctuation range is from 2.6

kHz to 20 kHz and the SPL is almost the same at frequency higher than 5 kHz. For SAN acoustic device, the ± 3 dB range is from 6.6 kHz to 20 kHz, which is 4 kHz narrower than the PCS acoustic device, and the SPL is continually increasing as the frequency increases. The mounting of the SPL with frequency increase has already been reported by several groups and theoretical investigations have also been conducted to explain this phenomenon²⁹⁻³². There is no significant SPL climbing feature seen for PCS acoustic source at high frequencies. Moreover, SPL mounting for the PCS acoustic device is seen at low frequencies with a gradient larger than the SAN acoustic device. The rapid climbing of SPL in low frequency range indicates good device performance since the SPL is raised to a higher level at a lower frequency.

The power applied to the devices and the highest normalized SPL generated are compared to consider the efficiency of the devices. For the PCS acoustic device, the highest SPL generated is 56 dB with an AC power consumption of 25 mW. For the SAN acoustic source, the highest SPL generated is 59 dB with an AC power consumption of 266 mW, i.e., the PCS acoustic device uses less than $1/10^{\text{th}}$ the power but gives out almost the same SPL compared to the SAN acoustic device. The power spectra for both the PCS acoustic device and the SAN acoustic device are normalized. The normalization is done by setting the sound collecting distance at 1 cm and the total power consumption at 1 W. Power spectra of both acoustic sources are shown in Fig. 7. The PCS acoustic device reaches a highest normalized SPL of 79 dB considering the power consumption of DC bias and 88 dB considering only the AC power. The highest normalized SPL for PCS acoustic device is 18 dB higher than the SAN acoustic device, which fits well with the calculated results of 16.5 dB, indicating an efficiency enhancement by a factor of approximately 7. Enhancing the efficiency of ETA acoustic devices may enable the application of such sound sources to portable devices, i.e., smartphones, laptops and tablets, etc.

Furthermore, the SPL and power spectra comparison between PCS acoustic devices are also made [Fig. 8]. These PCS devices are on different wafers or differ in terms of their positions on a same wafer. Fig. 8 illustrates fabrication reliability and device consistency. All three spectra are almost the same in terms of shape and SPL. The similarity in spectra of devices at different positions on the same wafer indicates good device consistency and the similarity of spectra of devices on different wafers at the same position means good fabrication reliability.

The time dependency of PCS acoustic devices is tested, as shown in Fig. 9. This test shows slight spectral change in the high frequency range. When measured soon after fabrication, the PCS acoustic device has a ± 3 dB fluctuation range starting from 2 kHz

to 20 kHz and a ± 2 dB fluctuation range starting from 4 kHz to 20 kHz.

E Simulation Results

Performances of both the PCS acoustic device and the SAN acoustic device are simulated [Fig. 10]. The false color in the figure represents the SPL of each point in the space. The size of the device and the voltage are set according to the experiment. The PCS acoustic device has a 20 dB higher SPL as compared to the SAN device at 1 kHz at 1 cm distance (Fig. 10 a, b). The PCS acoustic source has a 15 dB higher SPL as compared to the SAN device at 10 kHz at 1 cm (Fig. 10 c, d), which fits well with the experiment. SPL variation range of the PCS acoustic device is 5dB smaller than the SAN acoustic device for both 1 kHz simulation and 10 kHz simulation. A theoretical comparison is presented in Fig.10 (e), which shows a direct difference between the PCS acoustic device and the SAN acoustic device. It is clear from the result that the PCS acoustic device has a better performance, considering either maximum normalized SPL achieved or power spectrum flatness. A theoretical calculation up to 5 MHz of the PCS acoustic device is made, showing that the PCS acoustic device has an extremely flat frequency response at high frequency and a peak at around 18 kHz. The cause of the peak is possibly due to the point contact structure, whose surface-to-volume ratio is smaller than the SAN structure and makes the heat transfer process harder at high frequency.

F Conclusion:

A novel high performance point acoustic device was demonstrated. The fabrication is CMOS-compatible and wafer-scaled, enabling high throughput, miniaturization and circuit integration. Both PCS and SAN acoustic devices are compared in terms of the highest normalized SPL generated and the spectral fluctuation. It is found that the PCS acoustic device generates higher normalized SPL and has a flatter spectrum. The highest normalized SPL can reach 88 dB, which enhances the efficiency of the ETA device. As shown in Table 1, the PCS device is a more efficient wide-band ETA actuator as compared to the devices based on the materials and structures referred to in Table 1. The acoustic device can operate under flatness restriction within a broad range starting at a frequency around 2 kHz, which indicates a better performance than traditional ETA acoustic devices, and the response of the device is detectable at a frequency as low as 500 Hz. We expect that as pulse density modulation³⁵ is applied to the device, the proposed ETA device could be used for loudspeaker or earphone applications. Theoretical analyses and simulations are conducted, supporting the high efficiency and flat power spectrum features of PCS acoustic devices. Although popular transducers

(moving coil, electrostatic, and piezoelectric) are not typically CMOS-compatible, they produce larger SPL than an ETA device. The ETA device still need continuous improvements considering the efficiency in order to make it suitable for practical loudspeaker and headphone applications.

Acknowledgments

This work was supported by the National Natural Science Foundation (60936002, 61025021, 61434001, 61574083), the 973 Program (2015CB352100), the National Key Project of Science and Technology (2011ZX02403-002) and the Special Fund for Agroscientific Research in the Public Interest (201303107) of China. M.A.M is additionally supported by the Postdoctoral Fellowship (PDF) program of the Natural Sciences and Engineering Research Council (NSERC) of Canada and the China Postdoctoral Science Foundation (CPSF).

References

1. S.-S. Je, F. Rivas, R. E. Diaz, J. Kwon, J. Kim, B. Bakkaloglu, S. Kiaei and J. Chae, *Biomedical Circuits and Systems, IEEE Transactions on*, 2009, **3**, 348-358.
2. M.-C. Cheng, W.-S. Huang and S. R.-S. Huang, *Journal of Micromechanics and Microengineering*, 2004, **14**, 859.
3. H. Kim, S. Lee, S. Lee and K. Park, *Journal of Korean Physical Society*, 2009, **54**, 930.
4. Y.-P. Zhu, T.-L. Ren, Y. Yang, X.-M. Wu, N.-X. Zhang, L.-T. Liu and Z.-J. Li, 2006.
5. S. H. Yi and E. S. Kim, *Japanese journal of applied physics*, 2005, **44**, 3836.
6. S. H. Yi and E. S. Kim, 2002.
7. S. S. Lee, R. P. Ried and R. M. White, *Microelectromechanical Systems, Journal of*, 1996, **5**, 238-242.
8. R. C. Roberts, J. Du, A. O. Ong, D. Li, C. Zorman and N. C. Tien, 2007.
9. P. Rangsten, L. Smith, L. Rosengren and B. Hök, *Sensors and Actuators A: Physical*, 1996, **52**, 211-215.
10. R. Venkatasubramanian, *Nature*, 2010, **463**, 619-619.
11. F. Braun, *Annalen der Physik*, 1898, **301**, 358-360.
12. H. D. Arnold and I. B. Crandall, *Physical Review*, 1917, **10**, 22-38.
13. H. Shinoda, T. Nakajima, K. Ueno and N. Koshida, *Nature*, 1999, **400**, 853-855.
14. A. O. Niskanen, J. Hassel, M. Tikander, P. Maijala, L. Grönberg and P. Helistö, *Applied Physics Letters*, 2009, **95**, 163102.
15. H. Tian, C. Li, M. A. Mohammad, Y.-L. Cui, W.-T. Mi, Y. Yang, D. Xie and T.-L. Ren, *ACS nano*, 2014, **8**, 5883-5890.
16. H. Tian, T.-L. Ren, D. Xie, Y.-F. Wang, C.-J. Zhou, T.-T. Feng, D. Fu, Y. Yang, P.-G. Peng and L.-G. Wang, *ACS nano*, 2011,

- 5, 4878-4885.
17. H. Tian, D. Xie, Y. Yang, T.-L. Ren, Y.-F. Wang, C.-J. Zhou, P.-G. Peng, L.-G. Wang and L.-T. Liu, *Nanoscale*, 2012, **4**, 2272-2277.
 18. H. Tian, D. Xie, Y. Yang, T. L. Ren, Y. F. Wang, C. J. Zhou, P. G. Peng, L. G. Wang and L. T. Liu, *Nanoscale*, 2012, **4**, 3345-3349.
 19. C. Feng, K. Liu, J.-S. Wu, L. Liu, J.-S. Cheng, Y. Zhang, Y. Sun, Q. Li, S. Fan and K. Jiang, *Advanced Functional Materials*, 2010, **20**, 885-891.
 20. B. J. Mason, S.-W. Chang, J. Chen, S. B. Cronin and A. W. Bushmaker, *ACS nano*, 2015.
 21. Y. Wei, X. Lin, K. Jiang, P. Liu, Q. Li and S. Fan, *Nano Lett*, 2013, **13**, 4795-4801.
 22. A. E. Aliev, M. D. Lima, S. Fang and R. H. Baughman, *Nano letters*, 2010, **10**, 2374-2380.
 23. L. Xiao, P. Liu, L. Liu, Q. Li, Z. Feng, S. Fan and K. Jiang, *Journal of Applied Physics*, 2011, **110**, 084311.
 24. H. Tian, D. Xie, Y. Yang, T.-L. Ren, Y.-F. Wang, C.-J. Zhou, P.-G. Peng, L.-G. Wang and L.-T. Liu, *Applied Physics Letters*, 2011, **99**, 043503.
 25. H. Tian, D. Xie, Y. Yang, T.-L. Ren, Y.-X. Lin, Y. Chen, Y.-F. Wang, C.-J. Zhou, P.-G. Peng and L.-G. Wang, *Applied Physics Letters*, 2011, **99**, 253507.
 26. R. Dutta, B. Albee, W. E. van der Veer, T. Harville, K. C. Donovan, D. Papamoschou and R. M. Penner, *The Journal of Physical Chemistry C*, 2014, **118**, 29101-29107.
 27. T. Kihara, T. Harada and N. Koshida, *Sensors and Actuators A: Physical*, 2006, **125**, 422-428.
 28. S. S. Asadzadeh, A. Moosavi, C. Huynh and O. Saleki, *Journal of Applied Physics*, 2015, **117**, 095101.
 29. M. Daschewski, R. Boehm, J. Prager, M. Kreutzbruck and A. Harrer, *Journal of Applied Physics*, 2013, **114**, 114903.
 30. H. Hu, T. Zhu and J. Xu, *Applied Physics Letters*, 2010, **96**, 214101.
 31. C. W. Lim, L. H. Tong and Y. C. Li, *Journal of Sound and Vibration*, 2013, **332**, 5451-5461.
 32. H. Tian, D. Xie, Y. Yang, T. L. Ren, Y. F. Wang, C. J. Zhou, P. G. Peng, L. G. Wang and L. T. Liu, *Nanoscale*, 2012, **4**, 2272-2277.
 33. V. Vesterinen, A. O. Niskanen, J. Hassel and P. Helisto, *Nano Lett*, 2010, **10**, 5020-5024.
 34. M. N. Ozisik, *Heat conduction*, John Wiley & Sons, 1993.
 35. N. Koshida, A. Asami and B. Gelloz, 2008.

Attachment of:

A Point ETA Device Based on Aluminum Nanowires

Q.Xie et al.

Section I

Captions of Figures

Section II

Figures of Manuscript

Section III

Contents Entry

Captions of Figures

Attachment of:

A Point ETA Device Based on Aluminum Nanowires

Q.Xie et al.

Fig. 1 Schematic drawing of the heat transfer process of a) Traditional aluminum wire ETA device, b) SAN acoustic device, c) PCS device. a) Traditional devices suffer from severe heat leakage through the substrate as aluminum wires are fixed to the substrate. b) The design of SAN acoustic device weakens the heat leakage as there exists an air gap ($\sim 10 \mu\text{m}$) between the aluminum wires and the substrate. c) The design of PCS acoustic device solves the heat leakage problem by releasing the aluminum nanowires. The distance between the contact area and the substrate is $\sim 1 \text{ mm}$.

Fig. 2 a) Cross-section view of the PCS acoustic device. The contact area is released to about 1 mm above the substrate. b) Overview of wafer-scale PCS acoustic devices and SAN acoustic devices.

Fig. 3 Fabrication process of the PCS acoustic device. The SAN acoustic device shares the same process using different masks.

Fig. 4 Photos of, the a) PCS acoustic device after the lift-off process, and the b) SAN acoustic device after the lift-off process.

Fig. 5 Schematic drawings and SEM images of the device etching and releasing process. a) ~e): Enlarged and detailed etching process. The metallic top layer is aluminum, while the middle and bottom layers represent silicon oxide and silicon respectively. a) A part of the device before etching. b) Silicon oxide is etched. c) Due to the anisotropic nature of the ICP-RIE process, the silicon oxide layer under the aluminum is etched with a rate smaller than the rate of etching exposed silicon oxide. d) Silicon etching is conducted after the silicon substrate is exposed. e) Due to the anisotropic nature of the ICP-RIE process, the silicon layer under the silicon oxide is also etched. f) Schematic drawing of the device before etching. Interdigitated structure is shown. g) Schematic drawing of device after etching. Aluminum nanowires are released above the wafer. h) Overview of the PCS acoustic source. i) SEM photo of a PCS acoustic source device. The aluminum nanowires are curled and contact each other at a position above the substrate. j) A zoomed-in micrograph of the indicated area in panel (i). The marked area is the PCS. k) SEM photo of an SAN acoustic source device. l) A closer view of the SAN acoustic source device. The trapezoid structures are marked in panels (b) and (d).

Fig. 6 Schematic figure showing the test setup. Sound output is generated by the PCS acoustic device connected to a signal generator. Sound is captured by a microphone

and recorded by a dynamic signal analyzer. The signal generator and the signal analyzer are synthesized using an Agilent 35670A.

Fig. 7 Comparison between normalized performance of the PCS acoustic device and the SAN acoustic device. Both original spectra are normalized to 1 W AC input and 1 cm sound-collecting distance. The normalized PCS spectrum has a highest SPL 18 dB higher than the normalized SAN spectrum, indicating a more than 7 times enhancement of efficiency. The normalized spectrum of the PCS acoustic device is shifted to the average level of the normalized spectrum of the SAN acoustic device to compare the flatness. The normalized spectrum of PCS is flat (± 3 dB) from 2.6 kHz to 20 kHz, while the normalized spectrum of SAN is flat (± 3 dB) from 6.6 kHz to 20 kHz.

Fig. 8 Fabrication reliability and device consistency test of the PCS acoustic devices. The green line (GL) and red line (RL) correspond to sample 1 and 2 on the same wafer respectively, while the black line (BL) corresponds to sample 3 on another wafer whose relative position on the wafer is the same as sample 1. The level-consistency of the GL and RL indicates good device consistency whereas the shape-consistency and level-consistency of the RL and BL indicates good fabrication reliability.

Fig. 9 Time dependency of the PCS acoustic device. The device fabrication was performed on day 1 while day 8 is a week later. Immediately after fabrication, the device performs from as low as 1 kHz up to 20 kHz with a ± 3 dB range from 2 kHz to 20 kHz, and the SPL is uniform

from 4 kHz to 20 kHz. A week later the device is oxidized, showing slight changes in the spectrum.

Fig. 10 Simulations of SPL for SAN acoustic devices (a, c) and PCS acoustic devices (b, d) working at 1 kHz (a, b) and 10 kHz (c, d). The false color in a), b), c) and d) represent the SPL. The input power is the same for devices in a) and b), and c) and d), respectively. The PCS acoustic device generates higher SPL at both 1 kHz and 10 kHz. e) Comparison of theoretical performances between the PCS acoustic device and the SAN acoustic device. f) Power spectrum of the PCS acoustic device up to 5 MHz. It is shown that the PCS acoustic device has a flat power spectrum up to 5 MHz.

Table 1 Comparison of performances and features between different ETA devices.

Figures of Manuscript

Attachment of:

A Point ETA Device Based on Aluminum Nanowires

Q. Xie et al.

Fig. 1

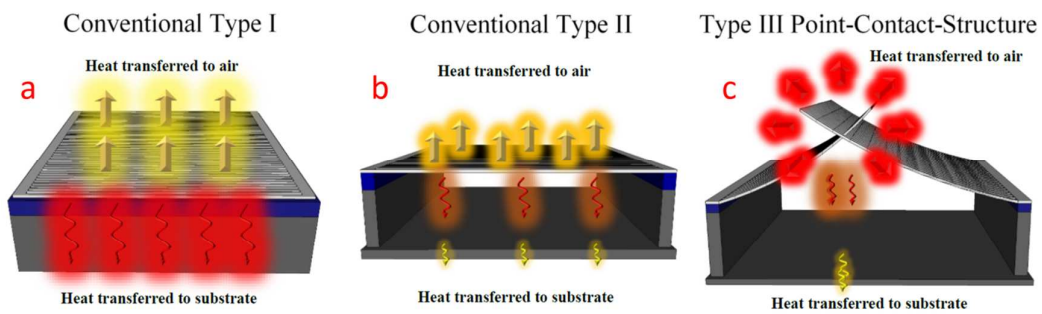


Fig. 2

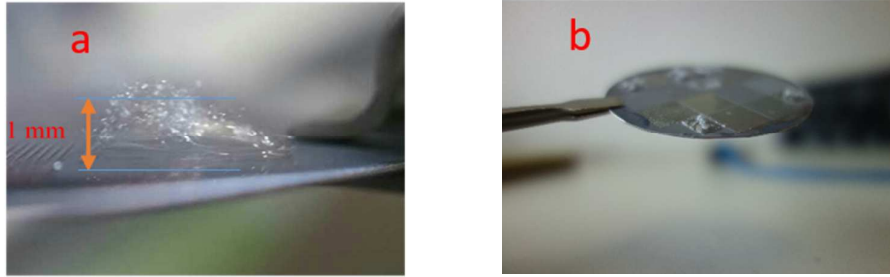


Fig. 3

Fabrication Process of PCS acoustic device

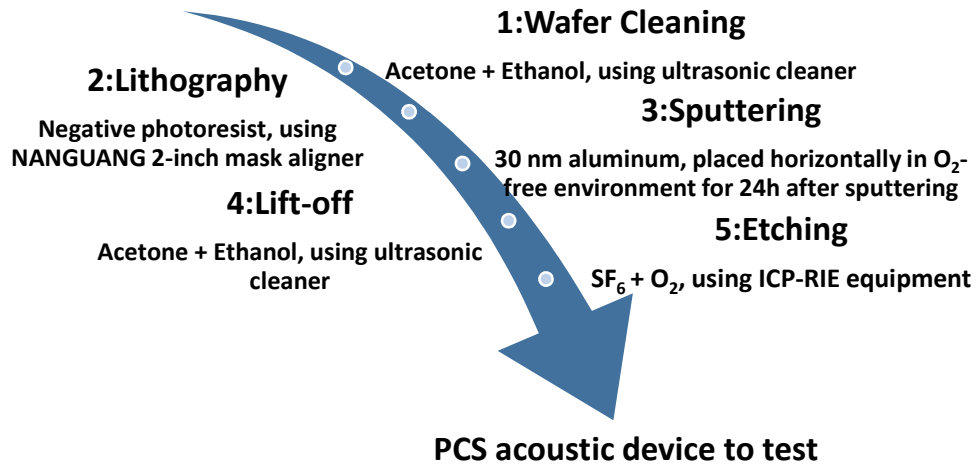


Fig. 4

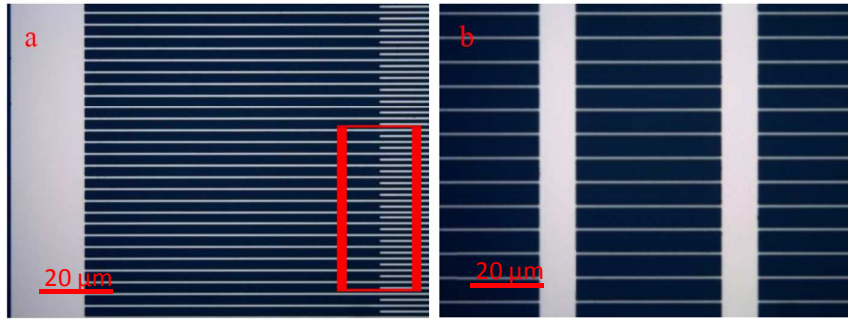


Fig. 5

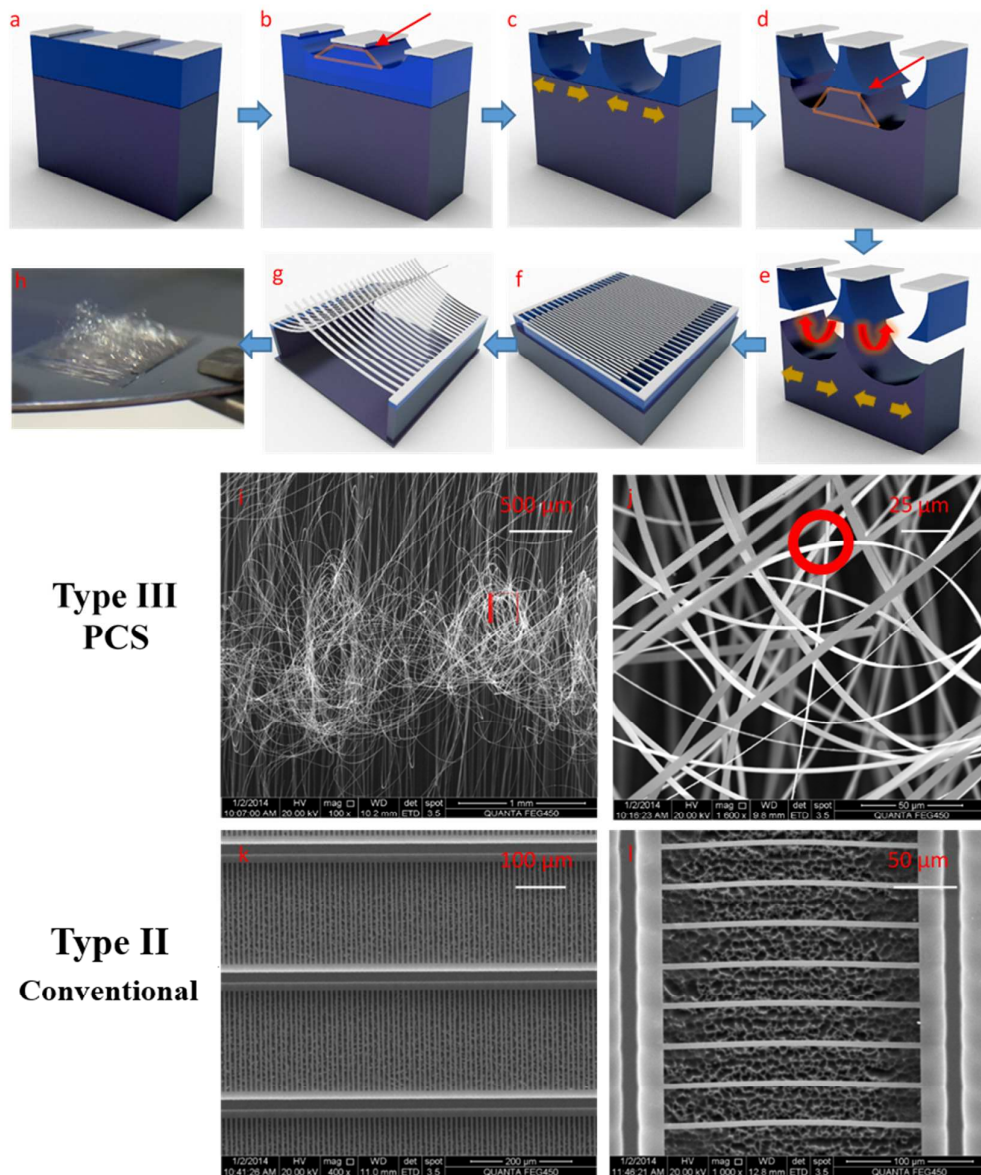
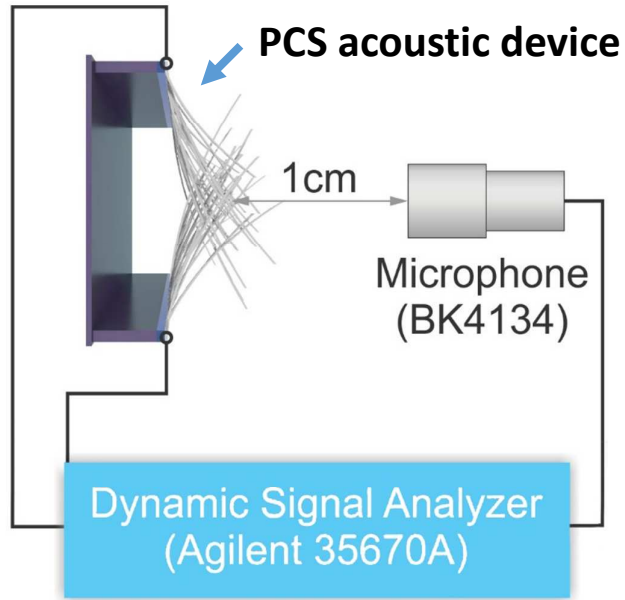
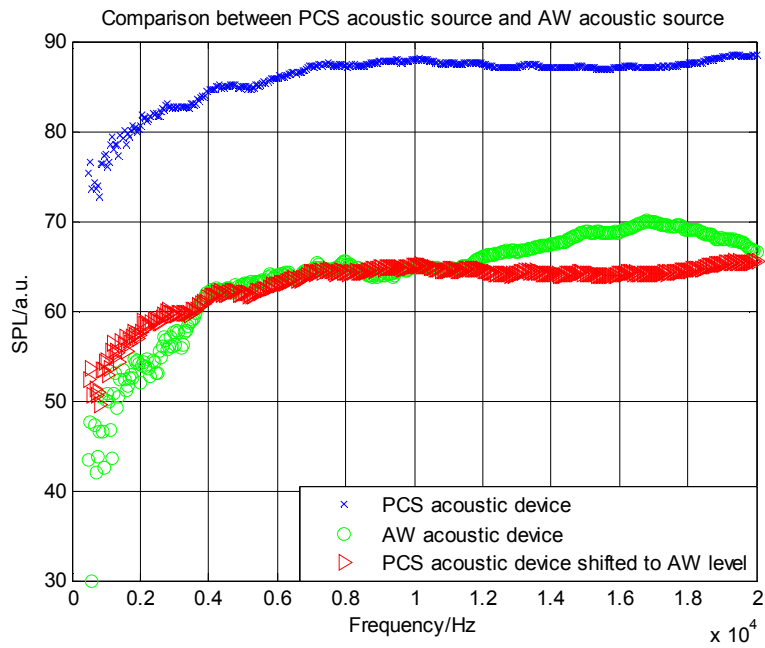


Fig. 6

**Fig. 7****Fig. 8**

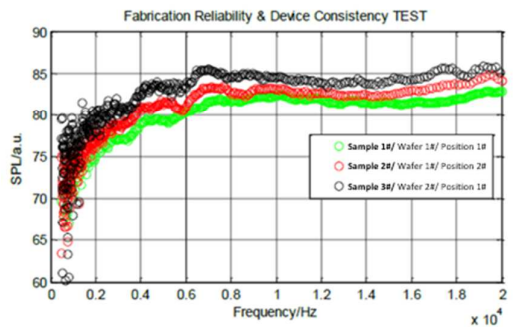


Fig. 9

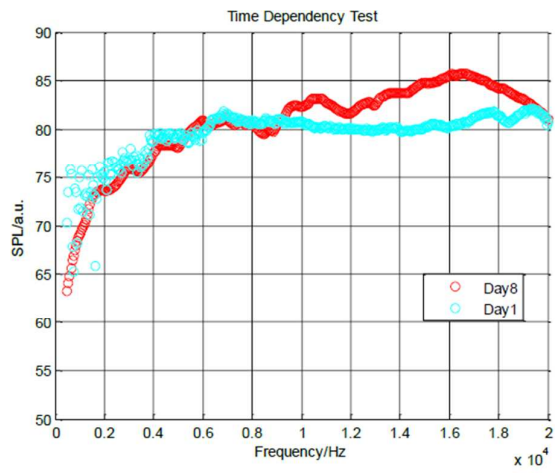


Fig. 10

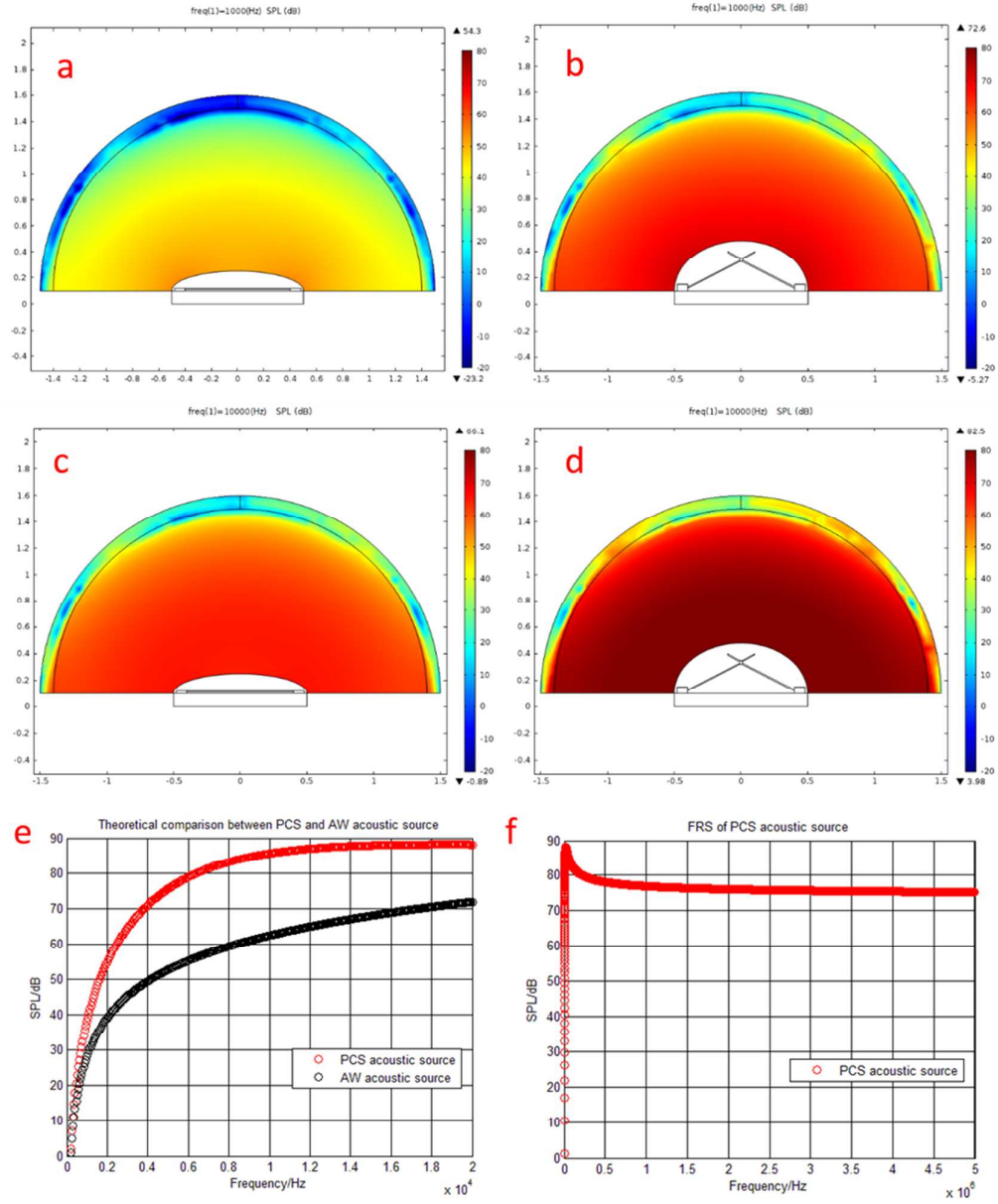
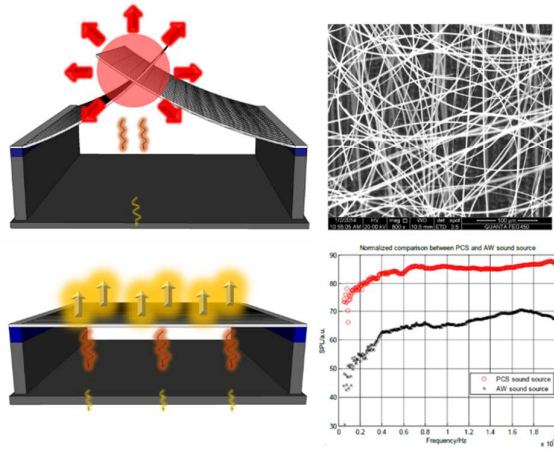


Table 1

Materials	SPL (dB)	2 kHz ~ 20 kHz fluctuation (dB)	Area (cm ²)	Reference
Reduced Graphene Oxide	35	± 15	1	6
Carbon Nanotubes	60	± 9	1	12
Suspended Al nanowires	79	± 11	17.5	5
PCS Al nanowires	88	± 3	0.3	This work

Contents Entry



The point-contact-structure minimizes the heat loss through the substrate and enhances the performance of the Electrical Thermal Acoustic devices.